Nonlinear AVO in the lab

Kris Innanen and Faranak Mahmoudian

ABSTRACT

The nonlinearity of the seismic amplitude-variation-with-offset (AVO) response in the presence of large relative changes in acoustic and elastic medium properties is investigated with physical modelling data. A procedure for pre-processing reflection data, acquired using the CREWES-University of Calgary physical modelling facility, is enacted on a reflection from a water/plexiglas boundary. The resulting picked and processed amplitudes are compared with exact solutions of the plane-wave Zoeppritz equations, as well as first, second, and third order $R_{\rm PP}$ approximations. We conclude that in the angle range $0 - 20^\circ$, the third order approximation is sufficient to capture the nonlinearity of the AVO response to within roughly 1% from a liquid-solid boundary with V_P, V_S and ρ contrasts of $1485 - 2745$m/s, $0 - 1380$m/s, and $1.00 - 1.19$gm/cc respectively. This is in contrast to the linear Aki-Richards approximation, which is in error by as much as 25% in the same angle range.

INTRODUCTION

Recently Innanen (2011, 2012) has presented analyses of nonlinear AVO modelling in situations of large relative change of elastic (or anelastic) parameters across a reflecting boundary. A key step in moving towards field application of such formulations lies in confirming their correct capture of real measurements. In this paper we compare the linear and nonlinear AVO approximations to physical modelling data.

The CREWES-University of Calgary physical modelling facility has been used to generate data sets from which AVO and AVAz responses of anisotropic targets can be examined (Mahmoudian et al., 2012). In carrying out that analysis, a pre-processing procedure was developed to correct picked reflection amplitudes for the laboratory, acquisition, and geometrical footprints in the data (a summary is provided in the following section). Here we enact this procedure upon the reflection from the water-plexiglas boundary.

Nonlinear plane-wave AVO approximations are derived, using the aforementioned approach, to conform to an acoustic incidence medium interrupted by an elastic target, and the known values of the density, P-wave and S-wave velocities of the water and plexiglas are used as input. The data and first, second, and third order AVO approximations based on the known elastic properties are compared over an angle range of $0 - 25^\circ$. The standard Aki-Richards approximation is computed from the CREWES Zoeppritz explorer and compared likewise.

Our overarching goal is to use these comparisons to establish the role nonlinearity may have to play in AVO as contrasts become large. To accomplish this, we organize this paper as follows. First, we review the physical modelling data set, its acquisition, and the pre-processing procedure. Second, we analyze the mathematical form of the exact P-P reflection coefficient associated with the shallowest reflector (which is an acoustic-elastic

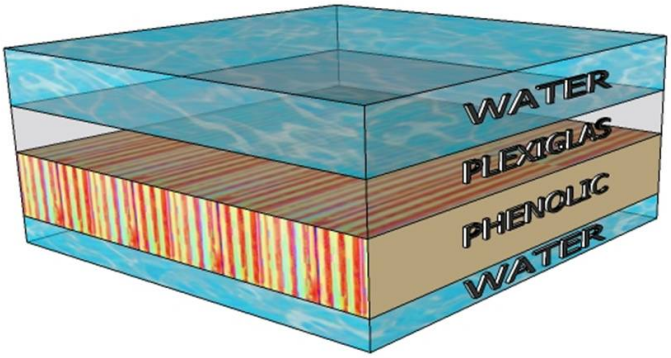

FIG. 1. The four-layered earth model used in physical modeling acquisition. The scaled thicknesses of water column and plexiglas layer are about 700m and 500m respectively.

boundary), deriving approximations to $R_{\rm PP}$ as functions of the relative changes $\Delta V_P/V_P$, $\Delta V_S/V_S$, and $\Delta\rho/\rho$. We lastly examine the accuracy of the approximations relative to our measured data and the exact $R_{\rm PP}$ curves, drawing conclusions about the ability of the third order corrected $R_{\rm PP}$ approximation to adequately capture AVO trends.

A PHYSICAL MODELLING DATA SET

A seismic physical model experiment has been conducted to acquire vertical-component reflection data over a four-layered model (Mahmoudian et al., 2012). The model consists of water and plexiglass, which are isotropic, and phenolic, which is a simulated fractured medium (see Figure 1). We will focus on the top two media in this paper, the elastic properties of which are included in Table 1.

Medium	V_P (m/s)	V_S (m/s)	ρ (gm/cc)
0	1485	~ 0	1.00
1	2745	1380	1.19

Table 1. Physical modelling medium elastic properties

A 2D vertical-component CMP gather of the data is shown in Figure 2. The target in this study is the earliest reflection, which is labelled A. A sequence of deterministic corrections are applied to the amplitudes picked on this event. In the remainder of this section we will summarize the corrections.

Amplitude preparation

Neither field nor laboratory recordings of seismic data directly indicate target reflection coefficients. The most important factors that disturb seismic amplitudes are: geometrical spreading, transmission loss, anelastic attenuation, interference of primary and ghost reflections, interbed multiples, and source/receiver array response, or *directivity* (e.g., Spratt et al., 1993). For the reflection labelled A in Figure 2, the relevant corrections are for geometrical spreading, emergence angle, and the source/receiver directivity. Because of the material types being used (water and plexiglas), attenuation may be neglected. The acquisition geometry was designed to avoid overlapping primary and ghost events, and the interference of multiples with event A.

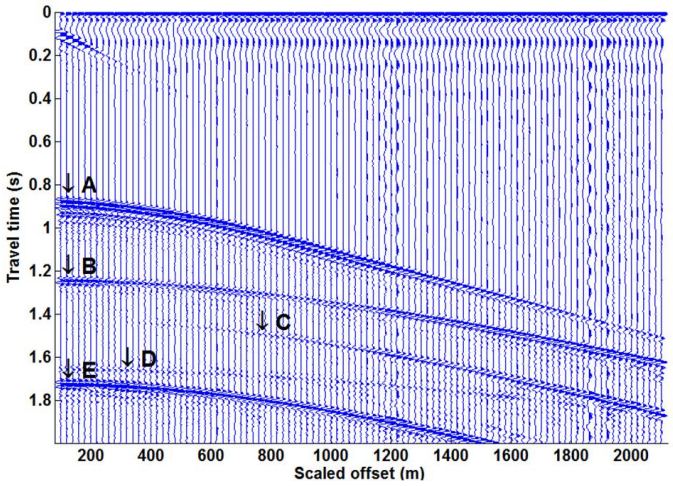

FIG. 2. A vertical-component CMP gather acquired over the four-layered model with a long gate automatic gain control applied. In the display, event "A" is the PP reflection from the water/plexiglas interface (our target), event "B" is the PP reflection from the top of the fractured layer), event "C" is the PS reflection from the top of the fractured layer, event "D" is the PP reflection from the bottom of the fractured layer, and event "E" is the PP reflection from the base layer.

The corrections are carried out as follows (for greater detail, see Mahmoudian et al., 2012):

1. *Geometrical spreading*. For a given offset and target depth, the primary ray-path is traced to determine the propagation radius. This radius is used to correct for geometrical spreading.

2. *Emergence angle*. Given the same inputs, P-P ray-tracing is also used to determine the emergence angle at the receiver location, through which the vertical recording is converted to total motion.

3. *Source/receiver directivity*. The source/receiver directivity correction compensates for the transducer radiation pattern in physical modelling acquisition; transducers when mapped to seismic scales are unphysical large.

The raw amplitudes picked on event A in Figure 2 are plotted in Figure 3 in light blue. In pink, green, and red are the cumulative results of the geometrical spreading correction, the emergence angle correction, and the directivity correction respectively. The red signal is our final pre-processed output. It is compared with the exact plane wave and spherical wave P-P solutions of the Zoeppritz equations in blue and black respectively.

In Figure 4a, the final form of the data set we will compare with AVO approximations is illustrated again; in Figure 4b we consider only the lower angle range $0 - 30^\circ$ which will be the focus of this paper.

NONLINEAR AVO MODELLING

Our objective is to examine the degree of AVO nonlinearity required to reproduce the AVO amplitudes and trend in Figure 4b. We will do this by adapting the approach of

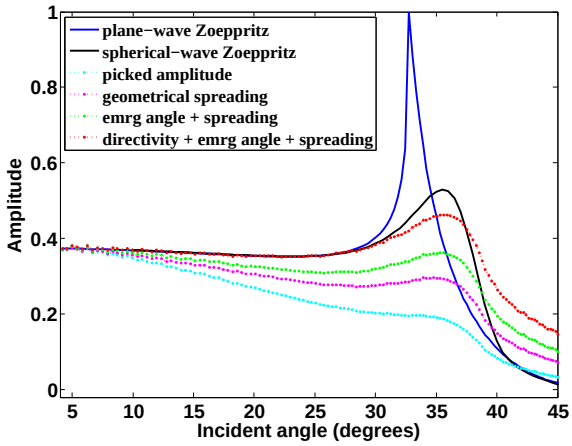

FIG. 3. Water-plexiglas reflection amplitudes corrected for geometrical spreading, emergence angle, and source/receiver directivity effects.

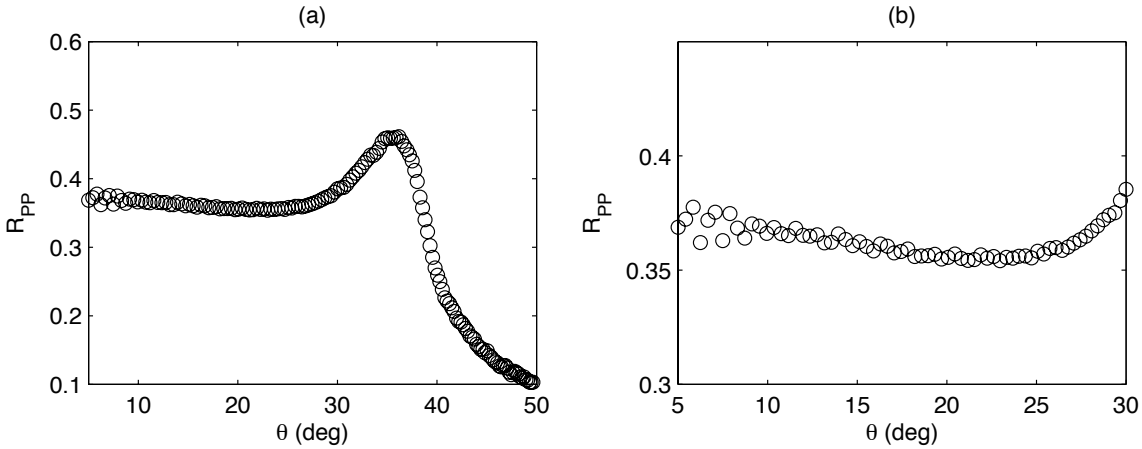

FIG. 4. Corrected $R_{\rm PP}$ values picked from the physical modelling reflection event A in Figure 2. (a) $R_{\rm PP}$ values for the full angle range; (b) $R_{\rm PP}$ values for the smaller angle range $0 - 30^\circ$ that constitutes the focus of the modelling in this paper.

Innanen (2012) to accommodate an acoustic incidence medium.

$R_{\rm PP}$ for water over an elastic half-space

The Zoeppritz equations (e.g., Aki and Richards, 2002; Keys, 1989), configured to represent a P-wave in an acoustic medium incident on an elastic target, may be solved for the P-P reflection coefficient $R_{\rm PP}(\theta)$ for small incidence angles θ as follows:

$$R_{\rm PP}(\theta) \approx \frac{AD(AC-1) + 4A^2D^3\,(D-C)\sin^2\theta - \frac{1}{2}ADC\,(A-C)\sin^2\theta}{AD(AC+1) + 4A^2D^3\,(D-C)\sin^2\theta - \frac{1}{2}ADC\,(A+C)\sin^2\theta}, \qquad (1)$$

where A–D are the ratios

$$A = \frac{\rho_1}{\rho_0}, \quad C = \frac{V_{P_1}}{V_{P_0}}, \quad D = \frac{V_{S_1}}{V_{P_0}}. \qquad (2)$$

Figure 5 illustrates the configuration, which matches the experimental arrangement discussed in the previous section.

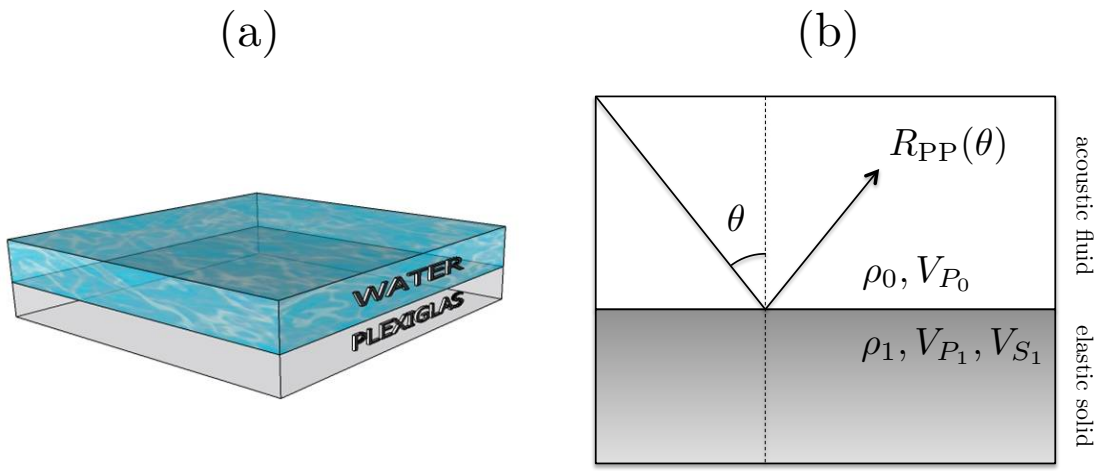

FIG. 5. Configuration of acoustic incidence medium/elastic target medium experiment. (a) We focus on the top two media used in the full physical modelling experiment illustrated in Figure 1. (b) The reflected P-P amplitude is modelled in terms of the acoustic and elastic properties above and below the interface.

Defining relative changes in parameters

We next define the relative changes in elastic parameters, maintaining the standard definitions (Castagna and Backus, 1993) whenever possible given the configuration in Figure 5. The relative change in P-wave velocity is defined as usual: in terms of the ratio C from equation (2):

$$\frac{\Delta V_P}{V_P} = 2\frac{V_{P_1} - V_{P_0}}{V_{P_1} + V_{P_0}} = 2\frac{1 - C^{-1}}{1 + C^{-1}}. \tag{3}$$

We solve for C and expand in orders of the relative change:

$$\begin{aligned} C &= \frac{1 + \left(\frac{1}{2}\frac{\Delta V_P}{V_P}\right)}{1 - \left(\frac{1}{2}\frac{\Delta V_P}{V_P}\right)} \\ &= 1 + \left(\frac{\Delta V_P}{V_P}\right) + \frac{1}{2}\left(\frac{\Delta V_P}{V_P}\right)^2 + \frac{1}{4}\left(\frac{\Delta V_P}{V_P}\right)^3 + \ldots \ . \end{aligned} \tag{4}$$

The relative change in V_S requires some adjustment from its standard definition. Here we measure its change relative to V_{P_0}. Together with the density relative change we have

$$\begin{aligned} \frac{\Delta V_S}{V_S} &= 2\frac{V_{S_1} - V_{P_0}}{V_{S_1} + V_{P_0}} \\ \frac{\Delta \rho}{\rho} &= 2\frac{\rho_1 - \rho_0}{\rho_1 + \rho_0}, \end{aligned} \tag{5}$$

which may be related to the ratios A and D via

$$\begin{aligned} A &= 1 + \left(\frac{\Delta\rho}{\rho}\right) + \frac{1}{2}\left(\frac{\Delta\rho}{\rho}\right)^2 + \frac{1}{4}\left(\frac{\Delta\rho}{\rho}\right)^3 + ... \\ D &= 1 + \left(\frac{\Delta V_S}{V_S}\right) + \frac{1}{2}\left(\frac{\Delta V_S}{V_S}\right)^2 + \frac{1}{4}\left(\frac{\Delta V_S}{V_S}\right)^3 + ... \ . \end{aligned} \tag{6}$$

In the next section we will substitute these series into equation (1), and perform a final expansion to produce our linear and nonlinear approximations.

Expansion in orders of $\frac{\Delta V_P}{V_P}$, $\frac{\Delta V_S}{V_S}$, and $\frac{\Delta\rho}{\rho}$

Substituting equations (4) and (6) into equation (1), we perform a final binomial expansion of the denominator (e.g., Innanen, 2011). Collecting terms of equal order in the three relative change measures of the previous section, we have

$$R_{\text{PP}}(\theta) = R_{\text{PP}}^{(1)}(\theta) + R_{\text{PP}}^{(2)}(\theta) + R_{\text{PP}}^{(3)}(\theta) + ..., \tag{7}$$

where the first order term, closely related to the Aki-Richards approximation, is

$$R_{\text{PP}}^{(1)}(\theta) = \frac{1}{2}\left(1 - 3\sin^2\theta\right)\frac{\Delta V_P}{V_P} + 2\sin^2\theta\frac{\Delta V_S}{V_S} + \frac{1}{2}\frac{\Delta\rho}{\rho}, \tag{8}$$

the second order corrective term is

$$R_{\text{PP}}^{(2)}(\theta) = \frac{3}{2}\sin^2\theta\left(\frac{\Delta V_P}{V_P}\right)^2 - 6\sin^2\theta\left(\frac{\Delta V_P}{V_P}\right)\left(\frac{\Delta V_S}{V_S}\right) + 5\sin^2\theta\left(\frac{\Delta V_S}{V_S}\right)^2, \tag{9}$$

and the third order corrective term is

$$\begin{aligned} R_{\text{PP}}^{(3)}(\theta) = &-\frac{1}{8}\left(\frac{\Delta V_P}{V_P}\right)^2\left(\frac{\Delta\rho}{\rho}\right) - \frac{1}{8}\left(\frac{\Delta\rho}{\rho}\right)^2\left(\frac{\Delta V_P}{V_P}\right) \\ &+ \left[\frac{13}{2}\left(\frac{\Delta V_S}{V_S}\right)^3 + \frac{1}{4}\left(\frac{\Delta V_P}{V_P}\right)^3 + \frac{3}{8}\left(\frac{\Delta V_P}{V_P}\right)\left(\frac{\Delta\rho}{\rho}\right)^2\right. \\ &+ \frac{3}{4}\left(\frac{\Delta V_P}{V_P}\right)^2\left(\frac{\Delta\rho}{\rho}\right) + \frac{5}{2}\left(\frac{\Delta V_S}{V_S}\right)\left(\frac{\Delta V_P}{V_P}\right)^2 \\ &- 9\left(\frac{\Delta V_S}{V_S}\right)^2\left(\frac{\Delta V_P}{V_P}\right) - \frac{1}{2}\left(\frac{\Delta\rho}{\rho}\right)^2\left(\frac{\Delta V_S}{V_S}\right) \\ &\left. - \left(\frac{\Delta V_P}{V_P}\right)\left(\frac{\Delta V_S}{V_S}\right)\left(\frac{\Delta\rho}{\rho}\right)\right]\sin^2\theta. \end{aligned} \tag{10}$$

These may be calculated to any desired order; we will stop at third order in this paper. Equation (7) is a forward modelling formula: given the acoustic and elastic properties of a real or notional experiment, the resulting R_{PP} values can be approximately calculated by truncating at . The higher order terms should return numerical accuracy to the modelling in situations of large contrast, while simultaneously maintaining the qualitative interpretability of the the Aki-Richards approximation.

RESULTS: NONLINEAR-APPROXIMATE VS. LABORATORY R_{PP}

In Table 1 the elastic properties of the media involved in the physical modelling experiment were enumerated. As a benchmark against which to evaluate our modelling, we use these properties as input in an independent calculation of the exact plane-wave R_{PP} and the standard Aki-Richards approximation*. Figure 6 illustrates the results.

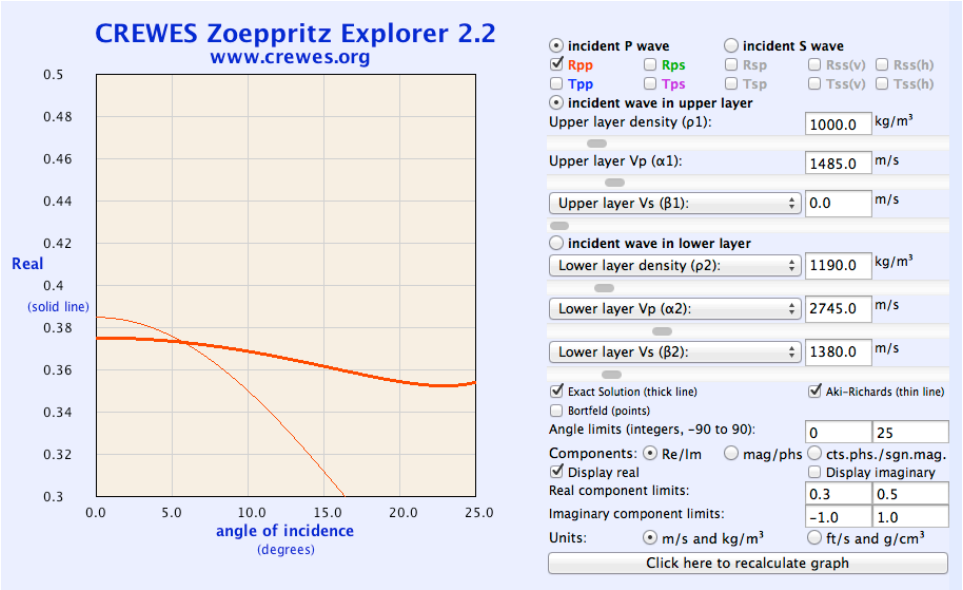

FIG. 6. Modelling using CREWES' Zoeppritz explorer. In bold orange is the exact $R_{\mathrm{PP}}(\theta)$ solution, and the thin orange line is the linearized Aki-Richards approximation.

In Figure 6, the bold orange line represents the exact plane-wave $R_{\mathrm{PP}}(\theta)$, and the thin orange line represents the Aki-Richards, or first order, approximate solution. The discrepancy between the two is a strong indication of the nonlinearity of the AVO response of this target, and suggests that the physical modelling data will be well-suited to test the effectiveness of the second and third order corrective terms in equations (7)–(10).

We assess the effectiveness of three truncations of equation (7) in turn. The results are summarized in Figure 7. In Figure 7a, the data after processing is plotted, with the exact solution (identical to the bold orange curve in Figure 6) overlain. In Figure 7b, the same data are plotted, with the linear approximate $R_{\mathrm{PP}}(\theta) \approx R^{(1)}_{\mathrm{PP}}(\theta)$ in blue. As we might expect, the curve is essentially identical to the Aki-Richards approximation in Figure 6. In reproducing the AVO signature of the plexiglas target, the linear approximation exhibits significant error in its capture of the angle trend and absolute values of the measured R_{PP} data. This re-emphasizes that the nonlinearity of the $\frac{\Delta V_P}{V_P}$, $\frac{\Delta V_S}{V_S}$, $\frac{\Delta \rho}{\rho}$ v. R_{PP} relationship takes a deciding role in this example.

In Figure 7c the second order approximation $R_{\mathrm{PP}}(\theta) \approx R^{(1)}_{\mathrm{PP}}(\theta) + R^{(2)}_{\mathrm{PP}}(\theta)$ is illustrated. There appears to be a significant difference in the reproduction of the AVO trend, but a

*The CREWES Zoeppritz Explorer 2.2 (C. Ursenbach, G. Margrave, E. Krebes) *http://www.crewes.org/ResearchLinks/ExplorerPrograms/*

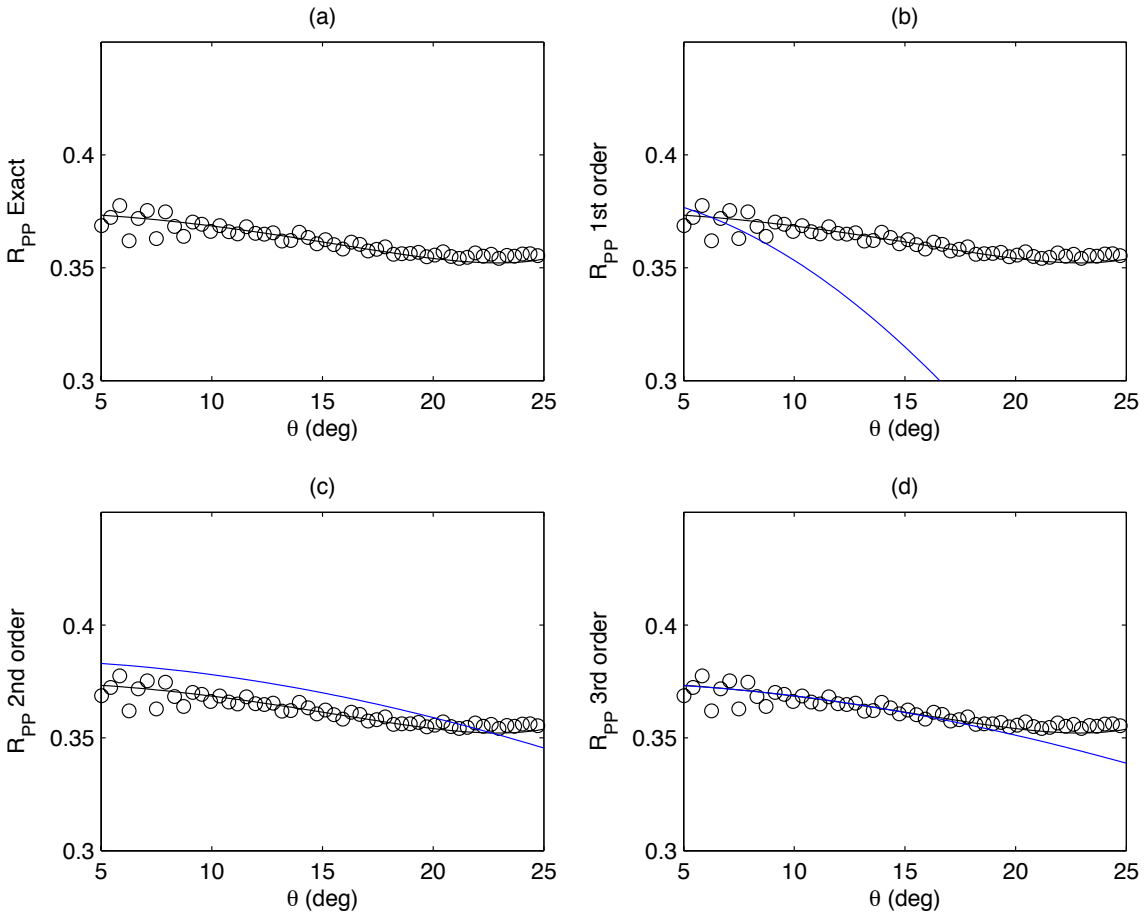

FIG. 7. Modelled data vs. lab data. (a) Exact solution for $R_{\rm PP}$ is plotted as a solid line, as are measured lab data. (b) First-order (linearized) $R_{\rm PP}$ approximation is plotted in blue against the same measurements. (c)-(d) Second- and third-order approximations plotted agains the lab data similarly.

remaining non negligible error in the absolute $R_{\rm PP}$ values. This is mathematically expected, since the second order term which effects this alteration, being proportional to $\sin^2\theta$, has no contribution at normal incidence. The absolute error in $R_{\rm PP}$ for angles up to 20° is then much more dramatically reduced in the third order approximation $R_{\rm PP}(\theta) \approx R^{(1)}_{\rm PP}(\theta) + R^{(2)}_{\rm PP}(\theta) + R^{(3)}_{\rm PP}(\theta)$, as illustrated in Figure 7d.

In Figure 8 we illustrate a simple quantification of these varying degrees of approximation error. In Figures 8a–c the percent error of the first, second, and third order approximations relative to the laboratory data are plotted. They are calculated as follows:

$$\%\ \text{error} = 100\% \times \frac{R^{\rm lab}_{\rm PP}(\theta) - R^{\rm approx}_{\rm PP}(\theta)}{R^{\rm lab}_{\rm PP}(\theta)}. \tag{11}$$

in Figures 8d–f the percent error relative to the exact plane-wave Zoeppritz solutions are likewise plotted. The first order (Aki-Richards) approximation is in error by roughly 50% at 25°. In contrast, at 25°, the second and third order approximations are in error by roughly 5%. However, the second order approximation displays this error over the whole angle range 0-25°, whereas the third order approximation exhibits a relative error of roughly 1%

from normal incidence to an angle of 20°.

Beyond 20°, the exact curve alters in character, beginning to follow a pattern with a degree of curvature more complicated than can be captured with terms proportional to $\sin^2\theta$. This behaviour being therefore at least second order in $\sin^2\theta$, is thus not expected to be reproduced by our particular approximation. Terms of order 2 and higher in $\sin^2\theta$ should be incorporated in equation (1) to increase the angle range over which the data are accurately fitted.

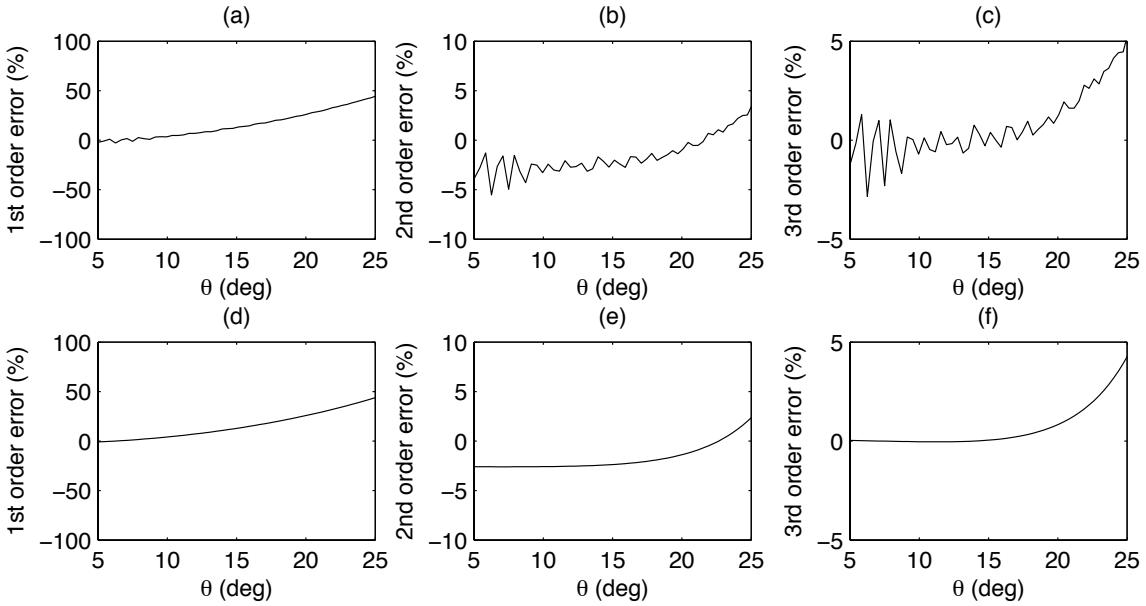

FIG. 8. Percent error of the AVO approximations relative to lab and exact synthetic R_{PP} curves. (a)–(c) Linear, second, and third order approximation error relative to the physical modelling lab data respectively; (d)–(f) linear, second, and third order approximation error relative to the exact synthetic R_{PP} data respectively.

CONCLUSIONS

Nonlinear AVO models are used to reproduce physical modelling lab data in large contrast, low angle scenarios. A procedure for processing the laboratory data to be comparable to plane-wave reflection coefficients is enacted and the results are compared with exact, first, second and third order R_{PP} approximations, whose forms are derived using recent nonlinear methods adapted to the acoustic-elastic character of the boundary.

The linear approximation (i.e., first order in the relative changes), which is equivalent to the Aki-Richards approximation, is seen have absolute amplitudes which are in error by as much as 25% within the range $0 - 25^\circ$, and to be unable to capture the AVO trend at any angle. Correcting the linearized AVO curve with the nonlinear second and third order terms reproduces the AVO response of a water-plexiglas boundary immersed in water up to 20° to within 1-2%. We consider this to be strong evidence that nonlinearity is a non-negligible, and in fact dominant, presence for acoustic/elastic contrasts of the kind in Table 1. Low order corrections to the Aki-Richards approximation can account for this nonlinearity, without losing the benefits associated with linearization (e.g., expression in terms of relative changes and qualitative interpretability).

ACKNOWLEDGEMENTS

Joe Wong led the acquisition of the physical modelling data, and Gary Margrave was a lead developer of the procedure for preparation of the reflection amplitudes. This work was funded by CREWES and NSERC. We thank in particular the sponsors of CREWES for continued support.

REFERENCES

Aki, K., and Richards, P. G., 2002, Quantitative Seismology: University Science Books, 2nd edn.

Castagna, J. P., and Backus, M., 1993, Offset-dependent reflectivity: theory and practice of AVO analysis: SEG.

Innanen, K. A., 2011, Inversion of the seismic AVF/AVA signatures of highly attenuative targets: Geophysics, **76**, No. 1, R1–R11.

Innanen, K. A., 2012, Elastic parameter coupling in AVO and the importance of the number $V_p/V_s = 2$: Submitted to Geophysics.

Keys, R. G., 1989, Polarity reversals in reflections from layered media: Geophysics, **54**, 900–905.

Mahmoudian, F., Wong, J., and and, G. F. M., 2012, Azimuthal avo over a simulated fractured medium: a physical modelling experiment: SEG Expanded Abstracts, **31**, 1–5.

Spratt, R. S., Goins, N. R., and Fitch, T. J., 1993, Pseudo-shear – the analysis of AVO, *in* Castagna, J. P., and Backus, M. M., Eds., Offset dependent reflectivity - theory and practice of AVO analysis, SEG Geophysical Investigation in Geophysics Series.